PCCP

Accepted Manuscript

ROYAL SOCIETY OF CHEMISTRY

www.rsc.org/pccp

Journal Name

ARTICLE

Solution-State Photophysics of N-Carbazolyl Benzoate Esters: Dual Emission and Order of States in Twisted Push-Pull Chromophores.

Received 00th January 20xx,
Accepted 00th January 20xx

DOI: 10.1039/x0xx00000x

www.rsc.org/

*Liubov M. Lifshits, Darya S. Budkina, Varun Singh, Sergey M. Matveev, Alexander N. Tarnovsky, and Jeremy K. Klosterman**

The stepwise photoinduced charge transfer in a series of N-carbazolyl benzoate ester push-pull chromophores has been studied in solution. Dual emission from the locally excited (LE, the lowest-energy singlet excited state of ^1L_b nature localized on the carbazole donor) and the highly polarized, intramolecular charge-transfer states of (pre)-twisted type (TICT states) is observed in non-polar and polar solvents. Ultrafast transient spectroscopy reveals that the excitation into the ^1L_b LE is followed by rapid (~ps) charge separation into an emissive TICT state. Excitation into the second singlet excited state localized on the carbazole (S_2) with ^1L_a nature, results in sub-100 fs population of both ^1L_b and TICT states.

Introduction

Organic chromophores are key components in molecular optoelectronic application organic light emitting diodes and photovoltaics.[1–3] Among the many chromophores available, carbazole and its many derivatives tower as essential functional building blocks due to their ideal photophysical properties, e.g. efficient emission, large band gaps and high triplet energies and synthetic accessibility.[4] Indeed, carbazole biphenyls (CBPs) are ubiquitous host materials.[5–9] As with most organic chromophores, the resulting bulk optoelectronic behaviors strongly depend on the local environment. Non-emissive excimers can form upon aggregation in the solid materials and serve as trap states that result in non-optimal device performance.[10–13]

Recently we reported enhanced solid-state emission from 5-(9H-carbazol-9-yl)-isophthlates incorporated within metal-organic frameworks (MOF) constructed of diamagnetic zinc ions.[14,15] Within the confines of the MOF, the carbazole ligands were rigidly held such to prevent cofacial overlap of adjacent carbazole π-systems and preclude quenching via non-emissive excimers. Furthermore, restricted rotation around the central C–N bond was hypothesized to impede formation of twisted intramolecular charge transfer (TICT) states.

Rettig[16–20] and others[21–24] showed that N-(4-cyanophenyl) carbazole in particular, along with many N-aryl carbazole derivatives but not N-phenyl carbazole, displayed broadened, highly solvatochromic emission indicative of a TICT state wherein the donor and acceptor moieties adopt a 90° conformation in the excited state. The Zachariasse[25,26] and Kapturkiewicz groups,[27–30] however, examined a series of N-aryl donor-acceptor carbazoles with cyano and keto electron withdrawing substituents and concluded that, although twisted, an orthogonal donor-acceptor TICT state was unlikely.

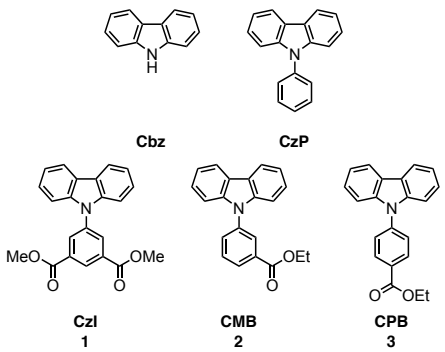

Fig. 1. Chemical structures of carbazole, **Cbz**, N-phenyl-carbazole, **CzP**, and push-pull carbazoles with dimethyl isophthalate, **CzI 1**, and ethyl benzoate acceptors **CMB 2** and **CPB 3**.

We now report the photophysical behavior of dimethyl 5-(9H-carbazol-9-yl) isophthalate **1** and two new analogues, ethyl 3-(9H-carbazol-9-yl) benzoate **2**, and ethyl 4-(9H-carbazol-9-yl) benzoate **3**, each with a single electron withdrawing ester groups (Fig. 1). X-ray crystallography and DFT calculations confirm a pre-twisted (θ ~ 50°) ground state structures retaining electronic communication between the two halves. Fluorescence spectroscopy reveals emission from localized carbazole LE states in the nonpolar cyclohexane and solvatochromic emission from twisted ICT states in increasing solvent polarity. Ultrafast transient absorption spectroscopy

[a] *Center for Photochemical Sciences, Department of Chemistry, Bowling Green State University, Bowling Green, Ohio, USA*

Electronic Supplementary Information (ESI) available: Crystallographic data, in CIF format, have been deposited with the Cambridge Crystallographic Data Centre (CCDC 1061880 and 1489317). Synthetic details, characterization, and analyses available online. See DOI: 10.1039/x0xx00000x

indicates that photoexcitation selectively accesses Frank Condon states, localized on the carbazole chromophore, which rapidly react, via electron transfer, to form the emissive Twisted ICT states.

Results and discussion

Absorption

The room temperature absorption spectra of **1**-**3** above 250 nm resemble that of N-phenyl carbazole with prominent bands at 290 nm and ~340 nm arising from the $^1L_a \leftarrow {}^1A$ and $^1L_b \leftarrow {}^1A$ transitions of carbazole, respectively (Fig 2). These $\pi \rightarrow \pi^*$ transitions are polarized in molecular plane along the respective long and short axis of carbazole.[31,32] The $\pi \rightarrow \pi^*$ transitions of the isophthalate and benzoate esters contribute to the intensity of the band at 290 nm.[33,34] Broad charge transfer (CT) bands appear as shoulders at 306 nm in **CzI 1** and at 314 nm for **CPB 3**, which confirms the push-pull nature of these new carbazole derivatives with increasing acceptor strength. **CzI 1**, due its greater electron withdrawing ability, also exhibits lower energy transitions at 352 nm. Although the *p*-benzoic ethyl ester of **CPB 3** possesses a single electron withdrawing ester, as compared to the two esters in isophthalate acceptor moiety of **CzI 1**, the charge transfer band at 314 nm is much more intense due to resonance.[16] The charge transfer band of the *m*-benzoic ester **CMB 2**, on the other hand, is effectively negligible as resonance is prohibited due to lack of orbital overlap. The intensity of the CT bands at ~310 nm shift to the blue and weaken with increasing solvent polarity. Here, increasing solvent polarity stabilizes the zwitterionic nature of the ground state and increases the contribution of CT transitions which lowers the overall band intensity as CT transitions typically display small oscillator strengths, due to poor orbital overlap.[35] A similar phenomenon has been previously observed in the CT absorption spectra of push-pull chromophores.[28]

Emission

Similar to previous 9-aryl carbazoles,[16,27–30] emission of carbazol-9-yl benzoic esters exhibit highly solvatochromic emission behavior; increasing the solvent polarity from cyclohexane to ethanol results in large red shifts and spectral broadening indicative of highly polarized TICT (twisted intramolecular charge-transfer) excited states (Fig. 3). As steric repulsion of hydrogens enforces a pre-twisted ground state conformation ($\theta \sim 50^\circ$) and prevents coplanarity in the excited state, we refer to this CT state as a twisted excited state (TICT), in accordance with earlier work.[16]

In nonpolar cyclohexane, the roughly structured emission of **CzI 1** in cyclohexane with broadened peaks at 377 and 390 nm closely resembles the emission of N-phenyl carbazole **CzP** but is red-shifted ~30 nm to lower energies due to the stabilization by the greater electron affinity and extended conjugation of the isophthalate acceptor. Fluorescence from N-phenyl carbazole is structured in both polar and non-polar

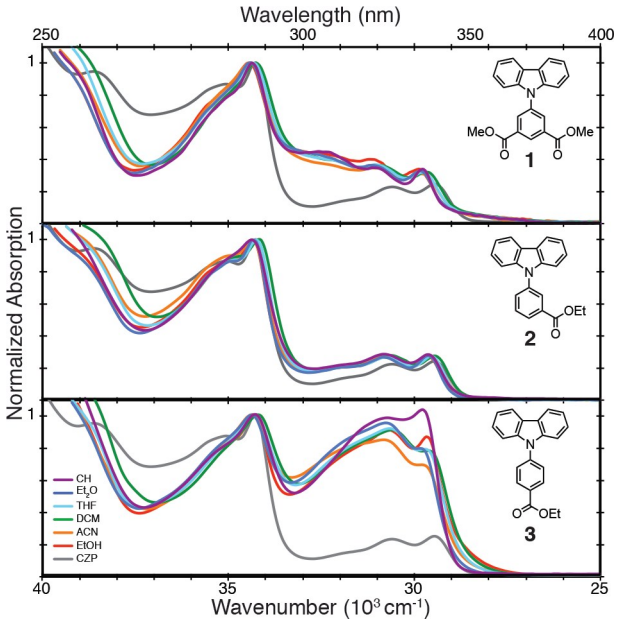

Fig. 2 Absorption spectra of 9H-carbazolyl benzoate esters **1**-**3** in cyclohexane (purple), diethyl ether (blue), tetrahydrofuran (cyan), dichloromethane (green), acetonitrile (orange) and ethanol (red) at room temperature. The absorption spectrum of **CzP** in acetonitrile is provided for comparison (grey).

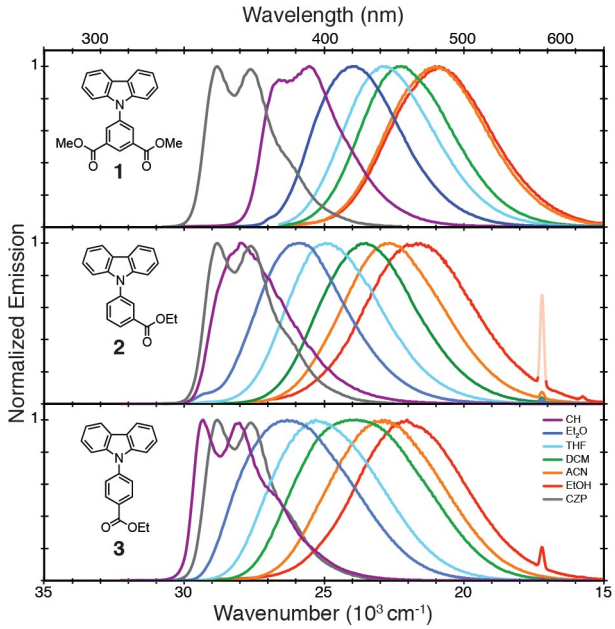

Fig. 3 Emission spectra of 9H-carbazolyl benzoates **1**-**3** in cyclohexane (purple), diethyl ether (blue), tetrahydrofuran (cyan), dichloromethane (green), acetonitrile (orange) and ethanol (red) at room temperature, λ_{ex} = 290 nm. Emission spectrum of **CzP** in acetonitrile is provided for comparison (grey). The second harmonic appears at 580 nm.

solvents and non-solvatochromic. Thus **CzP** emission has been attributed to the initially populated, locally excited (LE) state as excited state charge transfer does not occur.[16] We therefore refer to the structured emission band of **CzI 1** in cyclohexane as LE emission, in accordance with literature precedent.[36] The LE emission from **CMB 2** in cyclohexane is also broadened, but only slightly red-shifted, ~3 nm relative to **CzP** as the reduction

Table 1. Solvatochromic spectroscopic data of **1 – 3**: Absorption and emission maxima $\tilde{\nu}_a$ and $\tilde{\nu}_f$, Stokes shift $\Delta\tilde{\nu}$ and emission band full-width at half-maxima (fwhm$_f$) in wavenumbers (10^3 cm^{-1}).

	solvent	Δf^a	$\tilde{\nu}_a$ 10^3 cm^{-1}	$\tilde{\nu}_f$ 10^3 cm^{-1}	$\Delta\tilde{\nu}$ 10^3 cm^{-1}	fwhm$_f$[b] 10^3 cm^{-1}
1	CH	0.100	29.76	25.51	4.25	3.22
	Et_2O	0.256	29.85	23.92	5.93	3.60
	THF	0.308	29.76	22.78	6.98	3.72
	DCM	0.319	29.76	22.27	7.49	3.84
	ACN	0.393	29.85	21.05	8.80	5.64
	EtOH	0.379	29.85	20.88	8.97	4.35
2	CH	0.100	29.76	27.93	1.83	2.96
	Et_2O	0.256	29.76	25.84	3.92	3.70
	THF	0.308	29.85	24.94	4.91	3.92
	DCM	0.319	29.50	23.47	6.03	4.04
	ACN	0.393	29.59	22.68	6.91	4.22
	EtOH	0.379	29.67	21.60	8.08	4.54
3	CH	0.100	29.76	29.33	0.44	3.10
	Et_2O	0.256	29.85	26.32	3.54	4.74
	THF	0.308	29.67	25.32	4.36	3.59
	DCM	0.319	29.67	23.98	5.69	5.31
	ACN	0.393	29.85	22.88	6.97	4.72
	EtOH	0.379	29.76	22.03	7.74	4.53

[a] $\Delta f = \left(\frac{\varepsilon-1}{2\varepsilon+1}\right) - \left(\frac{n^2-1}{2n^2+1}\right)$ as defined in the text; [b] full width at half-maximum of emission

potential of the benzoate acceptor is less than that of isophthalate. Emission from **CPB 3** in cyclohexane, however, retains vibrational structure and is blue-shifted ~6 nm to higher energies. In polar acetonitrile, all compounds emit strongly from broad TICT bands centered at 475 nm, 441 nm, and 436 nm for **1 – 3**, respectively. Importantly, excitation spectra (Fig. S12, ESI†) indicate that the emissive LE and CT states are efficiently populated upon excitation into both the ^1L_a (λ_{ex} ~290 nm) and ^1L_b (λ_{ex} ~340 nm) states of carbazole in all the solvents irrespective of their polarity.

Excited State Dipole Moments

The emission wavelength maxima and Stokes shifts increase with increasing solvent polarity over the range of solvents examined. The solvent polarity dependence of the Stokes shift is related to the difference in the ground and excited state dipole moments by: [37,38]

$$hc(\tilde{\nu}_a - \tilde{\nu}_f) = hc(\tilde{\nu}_a^o - \tilde{\nu}_f^o) + \frac{2(\vec{\mu}_e - \vec{\mu}_g)^2}{a_o^3}\left[\frac{\varepsilon-1}{2\varepsilon+1} - \frac{n^2-1}{2n^2+1}\right] \quad (1)$$

where *h* is Planck's constant (erg·s), *c* is the speed of light (in cm^{-1}), $\tilde{\nu}_a$ and $\tilde{\nu}_f$ are the respective band positions of absorption and emission in wavenumbers (cm^{-1}), $\tilde{\nu}_a^o$ and $\tilde{\nu}_f^o$ are the respective extrapolated gas phase absorption and emission band positions (cm^{-1}), $\vec{\mu}_g$and $\vec{\mu}_e$are the respective dipole moments of the ground and excited states (in esu), a_0 is the radius of the Onsager cavity (in cm^{-1}),[39] ε is the solvent static dielectric constant,[40] and *n* is the solvent index of refraction. In cases where the absorption and emission transitions have

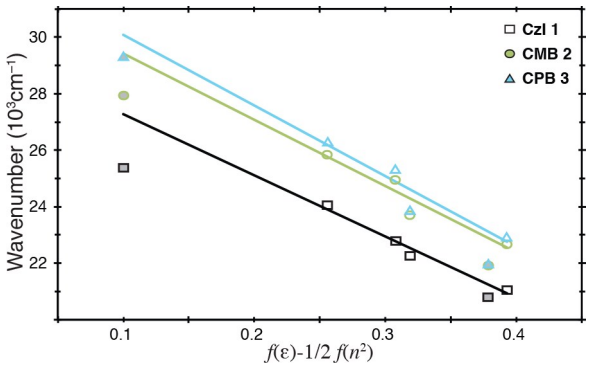

Fig. 4 Lippert-Mataga plots of TICT fluorescence maxima for **1 – 3** vs. solvent polarity $f(\varepsilon) - \frac{1}{2}f(n^2)$ for aprotic solvents CH, Et_2O, THF, DCM, and ACN.

Table 2. Onsager Radii, calculated ground state dipole moments, $\vec{\mu}_g$, and excited state dipole moments $\vec{\mu}_e$ estimated from solvatochromic plots of **1 – 3**:

			polar aprotic solvents			all solvents			
	a[a] Å	$\vec{\mu}_g$[b] D	$\frac{\mu_e(\mu_e-\mu_g)}{a_o^3}$ eV	R^2	$\vec{\mu}_e$ D	$\frac{\mu_e(\mu_e-\mu_g)}{a_o^3}$ eV	R^2	$\vec{\mu}_e$[a] D	$\vec{\mu}_e$[c] D
1	4.8	2.48[d]	1.34	0.98	16.7	0.99	0.93	14.5	15.4[d]
2	4.8	1.65[d]	1.45	0.91	16.9	1.23	0.92	15.6	15.6[d]
3	5.2	1.68	1.55	0.88	19.5	1.50	0.94	19.1	17.1

[a] where the Onsager radius *a* = 1/2 the length of the molecular axis [b] calculated using DFT (B3LYP/6-31G*).[c] calculated with TD DFT (B3LYP/6-31G*). [d]average dipole moment. (See ESI†)

different orbital origins, i.e. LE and CT states, it is advisable to simply use the fluorescence shift:[36]

$$hc\tilde{\nu}_f = hc\tilde{\nu}_f^o + \frac{2\vec{\mu}_e(\vec{\mu}_e - \vec{\mu}_g)}{a_o^3}\left[\frac{\varepsilon-1}{2\varepsilon+1} - \frac{1}{2}\frac{n^2-1}{2n^2+1}\right] \quad (2)$$

Lippert-Mataga plots of the CT emission maxima vs. Δ*f* for **1 – 3** show a linear relationship (average R^2 ≥ 0.93) (Fig. 4). Deviations from linearity, "data scatter," often arise from specific solvent-solute interactions, i.e. hydrogen bonding in EtOH.[40] For **CzI 1** and **CMB 2**, removal of the ethanol and cyclohexane data points from fitting significantly improved the correlation factors due to the difficulty in unambiguously separating the LE and CT contributions to emission in cyclohexane and hydrogen bonding in EtOH.[28] For **CPB 3**, excluding the EtOH and CH data points from fitting significantly lowered the correlation factors but did not affect the final calculated values (See ESI† for more details). Using the McRae solvent polarity function, which corrects for contributions of solvent-induced dipole moments, or Reichardt's normalized microscopic solvent polarity parameters also improved the fits (average R^2 ≥ 0.97 and 0.98, respectively) (See ESI†).[40] However, $\vec{\mu}_e(\vec{\mu}_e - \vec{\mu}_g)/a_o^3$ values from the slope of the Lippert-Mataga plots are more commonly employed and are used here to aid comparison of the excited state dipole moments within similar model frameworks.

From the solvatochromic slopes (Table 2), it is readily apparent that the emissive excited states are a) highly polarized (i.e. $\vec{\mu}_e \gg \vec{\mu}_g$); b) similarly stabilized by polar aprotic solvents; and c) comparable with related N-benzonitrilyl carbazoles (solvatochromic slopes of 1.35 – 1.51 eV).[25,28]

Table 3. Quantum Yields, Decay time, Radiative and non-radiative constants and transition dipole moments for **1 – 3.**

	Solvent	Φ_f	τ_f ns	k_f^o 10^7 s^{-1}	k_{nr} [b] 10^7 s^{-1}	M [c] D
1	CH	0.05	3.98	1.26	23.90	0.91
	Et_2O	0.10	13.00	0.79	6.91	0.85
	THF	0.15	21.16	0.73	3.99	0.83
	DCM	0.13	23.79	0.55	3.65	0.74
	ACN	0.11	25.33	0.44	3.51	0.78
	EtOH	0.04	12.25	0.33	7.84	0.67
2	CH	0.11	4.03	2.76	22.00	1.17
	Et_2O	0.15	8.69	1.71	9.80	1.14
	THF	0.28	16.52	1.71	4.34	1.12
	DCM	0.31	27.82	1.10	2.49	0.98
	ACN	0.32	36.23	0.88	1.88	1.00
	EtOH	0.04	8.71	0.49	11.02	0.76
3	CH	0.55	4.60	12.0	9.73	2.28
	Et_2O	0.58	5.48	10.6	7.68	2.74
	THF	0.80	7.59	10.6	2.59	2.73
	DCM	0.72	9.98	7.18	2.84	2.40
	ACN	0.60	12.48	4.79	3.23	2.29
	EtOH	0.23	5.21	4.41	14.78	2.29

[a] Excited at 340 nm and recorded at λ_{max}. [b] $k_f = \Phi_f/\tau$, and $k_{nr} = (1 - \Phi_f)/\tau$.

Calculation of estimated excited state dipole moments using eq. (4) is highly dependent[25] on the selection of *a*, the Onsager radius, and multiple methods for deriving spherical approximation of non-spherical molecules have been proposed (See ESI†).[22,26,41,42] Using half the length of the long molecular axis (as measured from single crystal X-ray structures) and ground state dipole moments, $\vec{\mu}_g$, determined using DFT calculations, excited state dipole moments of 17 – 20 D are obtained (Table 2). These large values suggest that full electron transfer from the carbazole nitrogen atom occurs to roughly the center of the aromatic benzoate acceptors upon excitation of **1 – 3**.[36] Excited dipole moments calculated from the Stokes shifts are quite similar (See ESI†). Excited state dipole moments from TD DFT calculations (see computational section) are similar in magnitude and trend.

Quantum Yields

Quantum yields of 9H-carbazolyl benzoate esters **1 – 3** gradually increase with greater solvent polarity but level off at THF (Δf = 0.308) potentially indicating dielectric saturation or, more likely, the concurrent stabilization of competitive non-radiative pathways (Table 3).[43–45] **CPB 3** is highly emissive, Φ_f = 55 to 80% whereas **CzI 1** and **CMB 2** are weakly and moderately emissive, 5 to 10% and 10 to 30% respectively. For all three compounds, emission decreases in EtOH, relative to the less polar ACN and THF. Specific solute-solvent interactions in protic solvents, i.e. ethanol, are well-established,[36] and hydrogen bonding interactions often augment non-radiative decay processes resulting in quenched emission.

Radiative Rates

Lifetimes of **CzI 1** and **CMB 2** range from 4 to 25 and 36 ns, respectively, whereas the lifetime of **3** only reaches 12.5 ns in ACN. As expected from the quantum yields, hydrogen-bonding interactions result in shortened lifetimes for **1 – 3** in ethanol. The radiative rate constants of **CzI 1** and **CMB 2**, calculated from $k_f^o = \phi_f/\tau_f$ with the assumption that irreversible formation of the emissive species occurs with 100% efficiency, are lesser than the radiative rates of **CPB 3**. The small k_f^o rate constants, particularly in the case of **1** and **2**, strongly indicate efficient charge separation in the emissive CT state, as compared to the nonpolar LE and ground states. In all cases the radiative rates decrease with increasing solvent polarity (~3 fold in acetonitrile), characteristic of a forbidden $S_o \leftarrow {}^1CT$ radiative transition between a largely decoupled, i.e. significantly (pre-) twisted, donor-acceptor pair.[16,46,28,47–49] The electronic transition dipole moments, M, as calculated according eq (3) decrease slightly with increasing solvent polarity. The small magnitude of the M values are typical of twisted intramolecular CT states.[36,50]

$$k_f = \frac{64\pi^4}{3h} n^3 \tilde{\nu}_f^3 |M|^2 \qquad (3)$$

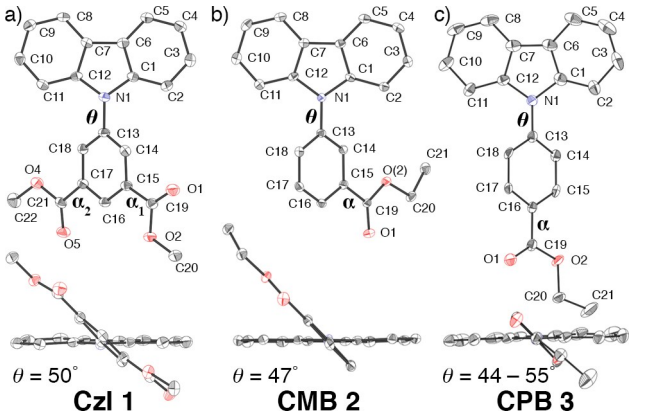

Fig. 5. Representative ORTEP plots of a) **CzI 1**, b) **CMB 2**, and c) **CPB 3** at 50% probability with numbering schemes and side view showing the twist angle between planes of the donor carbazole and acceptor isophthalate/benzoates. Hydrogen atoms have been omitted for clarity.

X-ray Crystal Structures of CzI 1, CMB 2 and CPB 3

Single crystals of **CMB 2** and **CPB 3** were obtained by slow evaporation of saturated solutions and analysed by X-ray diffraction.‡ The structural solution for **CPB 3** was non-trivial and will be reported shortly elsewhere.[51] The crystal structure of **CzI 1** was previously reported.[14] All of the push-pull chromophores are non-planar, due to steric repulsions, and adopt a twisted conformation with angles (θ) of 49.5˚, 47.5˚, and 44 – 55˚, between the best-fit planes of the donor-carbazole and acceptor isophthalate/benzoate ring atoms (Fig. 5). For **CMB 2** the ethyl ester is effectively coplanar whereas ester groups in **CzI 1** and **CPB 3** display slightly larger deviations from co-planarity (α = 6.70/7.21˚, 1.31˚, and ~ 9.52˚ for **1 – 3** respectively). Bond distances and angles are similar to other N-aryl substituted carbazoles and no strong indications of ground state CT interactions are apparent (Table S14, ESI†).[25,11,52–55]

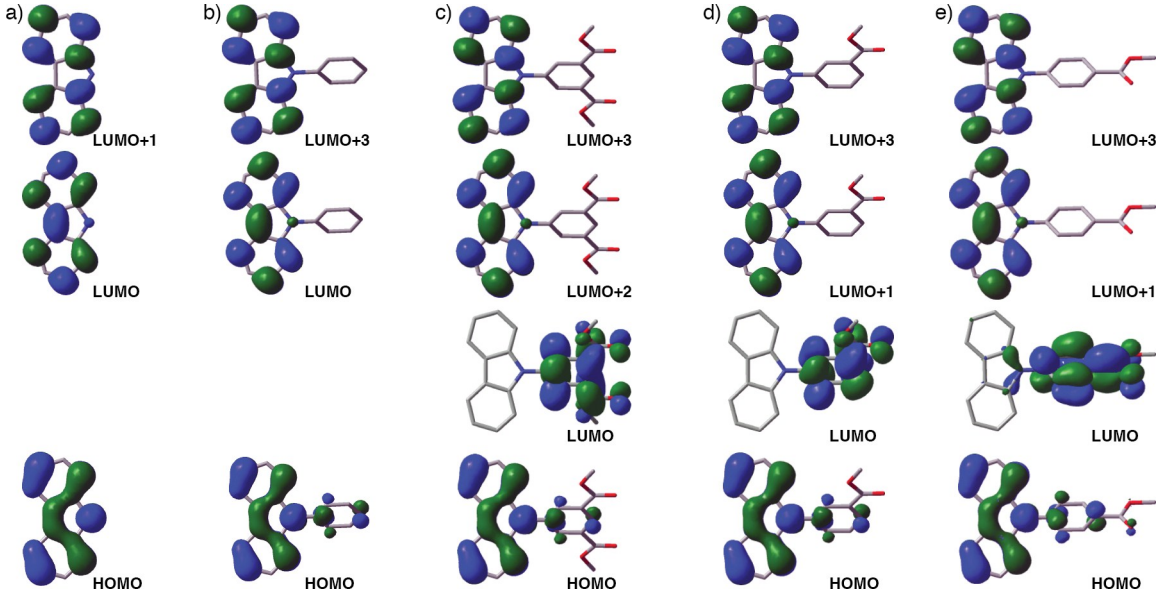

Fig. 6. HOMO, LUMO and relevant frontier molecular orbital diagrams (DFT B3LYP/6-31G*) for a) carbazole **Cbz**), b) N-phenyl carbazole (**CzP**), c) **CzI 1**,-*syn away* - conformer and the methoxy esters of d) **CMB OMe 2'** - *away* – conformer and e) **CPB OMe 3'**. Hydrogen atoms have been omitted for clarity.

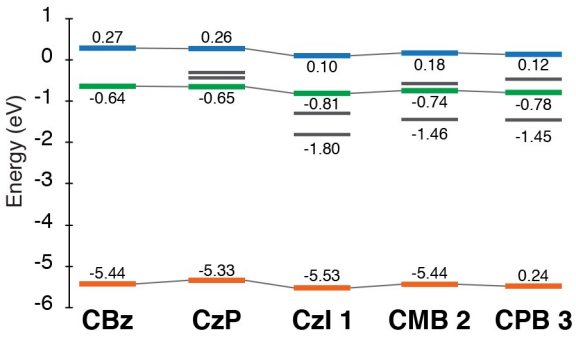

Fig. 7. HOMO, LUMO and relevant LUMO+*n* gas-phase energies (DFT B3LYP/6-31G*) of carbazole (**Cbz**), N-phenyl carbazole (**CzP**), and lowest energy conformers of 9*H*-carbazolyl methyl benzoates **1** – **3**. MOs corresponding to the **Cbz** ^1L_a and ^1L_b states are highlighted in blue and green, respectively.

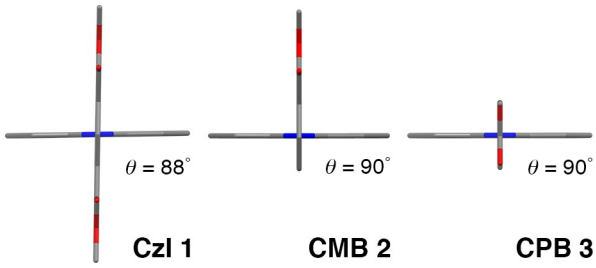

Fig. 8. Side view showing the twist angle between planes of the donor carbazole and acceptor isophthalate/benzoates in the optimized first excited state (TD DFT B3LYP/6-31G*) of **CzI 1**, **CMB OMe 2'**, and **CPB OMe 3'**. Hydrogen atoms omitted for clarity.

DFT Calculations

DFT calculations (B3LYP/6-31G*) generated non-planar, twisted ground state conformations for 9H-carbazolyl benzoate methyl esters of **1-3**, twist angles (θ) of 54.9˚, 54.7˚ and 52.0˚, respectively, which correspond well to the observed X-ray crystal structures (Fig. 6). The ester groups are effectively coplanar (α = ~0.9˚ for **1** – **3**, respectively). The calculated ground state dipole moments[56] align towards the vector of the non-carbonyl ester oxygen atom and are, therefore, strongly dependent on the orientation of the ester substituents; the dipole moment of the crystallographically observed *anti*-conformation of **1** is 1.75 D whereas the dipole moment of the favored solution state *syn*- conformers[57–59] are 2.14 and 3.55 D (Fig. S23 and Table S15, ESI†). The calculated dipole moments of the meta- **CMB 2** conformers are 0.40 and 2.90 D. The dipole moment of **CPB 3** is 1.68 D.

Orbital density in the HOMOs of **1** – **3** is located primarily on the electron rich carbazole moiety but can also be found at the *ortho* and *para* positions on the isophthalate/benzoate rings indicating ground state electronic coupling between the two halves (Fig. 6). In the case of **3**, electron density is also found on carbonyl oxygen of the para- ester groups. Population densities of the LUMOs are almost completely localized on the isophthalate/benzoate halves for **1** and **2**. The LUMO of **CPB 3**, however, extends from the central pyrrole ring to the acceptor benzoate indicating CT interactions. These results are consistent with the presence of CT bands strongly contributing to the absorption spectra of **3**, but only weakly present for **1** and **2** (Fig. 2). Comparison to the frontier orbitals of **Cbz** and **CzP** enables the identification of the carbazole ^1L_b state (LUMO for **Cbz** and **CzP**) as LUMO+2 for **1** and LUMO+1 for **2** and **3**. The carbazole ^1L_a state (LUMO+1 for **Cbz**, LUMO+3 for **CzP**) is now the LUMO+3 for **1**, **2** and **3**. The energies of these states remain fairly constant across the series (Fig. 7) and correspond to Franck-Condon excitation into the **Cbz** ^1L_b and ^1L_a states at 340 nm and 290 nm, respectively.

Optimization of the first excited states using single-point time-dependent DFT (TD DFT) calculations (B3LYP/6-31G*)[60–62]

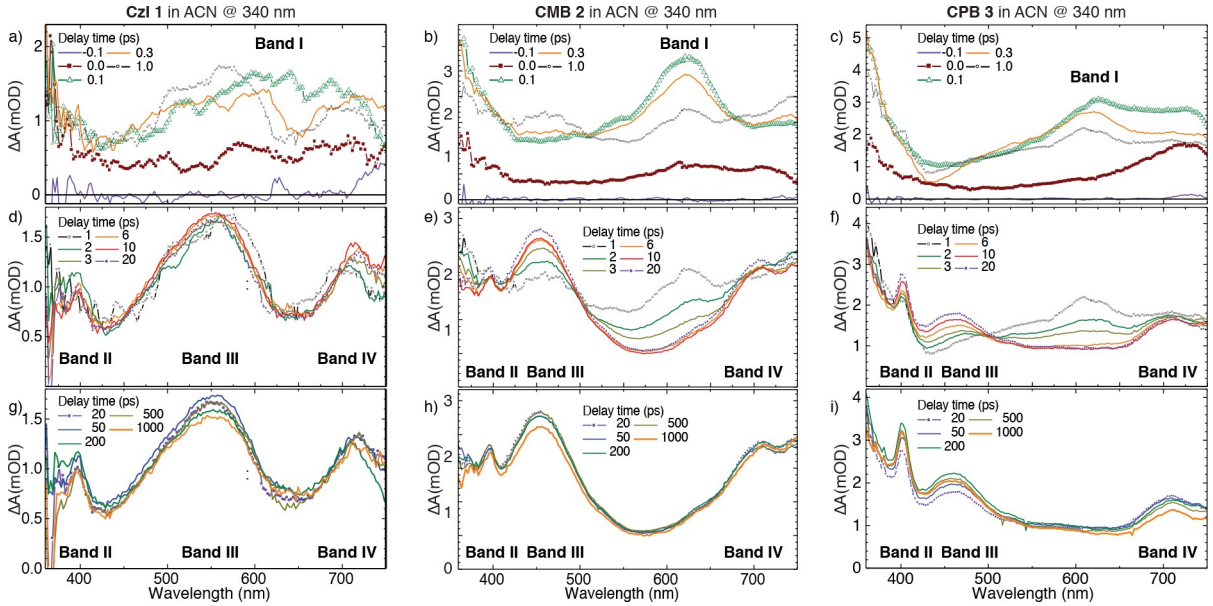

Fig. 9 Δ*A* spectra of **CzI 1**, **CMB 2** and **CPB 3** in a 0.1-mm flowing jet of acetonitrile at a – c) 0–1 ps, d – e) 1–20 ps and f– h) 20–1000 ps. Excitation at 340 nm (pulse energy, **5.3** *μJ*). Delay times between the excitation and probe pulses (in picoseconds) are shown in the legends.

Table 4 Parameters obtained from global fit analyses of transient absorption spectra of **CzI 1**, **CMB 2** and **CPB 3** in acetonitrile upon excitation at 340 and 288 nm.

	CzI 1				**CMB 2**				**CPB 3**			
	λ_{ex} 340 nm		λ_{ex} 288 nm		λ_{ex} 340 nm		λ_{ex} = 288 nm		λ_{ex} 340 nm		λ_{exc} 288 nm	
	τ_g / ps	ε^1 /nm	τ_g /ps	ε^1 / nm	τ_g / ps	ε^1 / nm	τ_g / ps	ε^1 / nm	τ_g / ps	ε^1 / nm	τ_g / ps	ε^1 / nm
τ_{0g}			0.096	412, 537			0.072	384, 613, 744			0.076	399, 717
τ_{1g}	0.07	640	0.18	600, 697	0.10	619	0.17	611	0.11	637, 723	0.15	620
τ_{2g}	1.40	594, 703	2.24	401, 567–586, 717	1.45	624	1.69	394, 477, 616, 725	1.65	616	2.1	595, 717
τ_{3g}	27	398, 562, 714	19	404, 566, 704	36	399, 457, 712	31	400, 461, 707	42	404, 466, 711	17	405, 468, 720
final[2]		396, 558, 711		399, 557, 712		399, 456, 706		400, 458, 701		403, 463, 713		403, 461, 707

[1] ε band maxima of evolution-associated difference spectra from the global fit, [2] permanent spectrum.

revealed relaxation into fully perpendicular geometries (θ = 88.2˚, 90.0˚, and 90.0˚, for the methyl esters of **1** – **3**, respectively) (Fig. 9 and Table S16, ESI†). The esters are nearly perfectly coplanar (α = 0.0˚ – 0.2˚). The orthogonal conformation greatly stabilizes the LUMOs (-0.54 to -0.62 eV relative to the GS) localized on the isophthalate/benzoate acceptor, lending credence to a twisted intramolecular CT state. The calculated excited state dipole moments of 12.8–18.0 for the conformers of **CzI 1**, 14.6 and 16.6 for **CMB 2**, and 17.1 D for **CPB 3**, are consistent with the experimental dipole moments calculated from the solvatochromic emission plots (Fig. 4).[63] The HOMO→LUMO transitions, directly leading to ICT, are forbidden ($f \sim 10^{-4}$), whereas the $S_o \rightarrow {}^1L_b$ transitions are partially allowed ($f \sim 0.04$) (Table S17, ESI†). These results are consistent with excitation primarily localized on the carbazole moiety, which then relaxes into a twisted ICT state.

Transient Absorption Measurements

Acetonitrile Solutions Two sets of measurements (at different excitation wavelengths) on **CzI 1**, **CMB 2**, and **CPB 3** were performed in acetonitrile solutions. Any noticeable transient absorption (Δ*A*) signals from neat acetonitrile occurred at delay times between −50 and 50 fs. Starting from a 100 fs delay time, the reported Δ*A* signals are due to excitation of **CzI 1**, **CMB 2**, and **CPB 3**.

Excitation at 340 nm In the first measurement set, solutions of **CzI 1**, **CMB 2**, and **CPB 3** in acetonitrile were excited at 340 nm, corresponding to the carbazole $S_0 \rightarrow {}^1L_b$ transition. This excitation wavelength was selected at the red edge of the UV-vis absorption spectra of these molecules to minimize excess vibrational energy in the S_1 (^1L_b) state. The spectral and temporal evolution of ΔA signals at short – (0.1 – 0.5 ps) and intermediate (0.5 – 20 ps) delay times between excitation and probe pulses is similar for all three compounds (Fig. 9). At 100 fs, intense transient absorption bands are centered at 600 – 620 nm (Band I). These bands undergo spectral narrowing within 200 fs, and then decay on a time scale of 2 ps with the formation of three transient absorption bands. Band II is centered at ~ 400 nm (sharp) and Band IV at ~ 700 nm (broad) for all three molecules. Band III is located at ~ 550 nm for **CzI 1** and ~ 470 nm for both **CMB 2** and **CPB 3**. For **CzI 1** and **CMB 2**, Bands II – IV remain without changes, within experimental accuracy, to the end of the measurement (1.2 ns). For **CPB 3**, Band IV at 700 nm decays slightly from 20 to 200 ps while absorptions below 590 nm, including Bands II & III, slightly

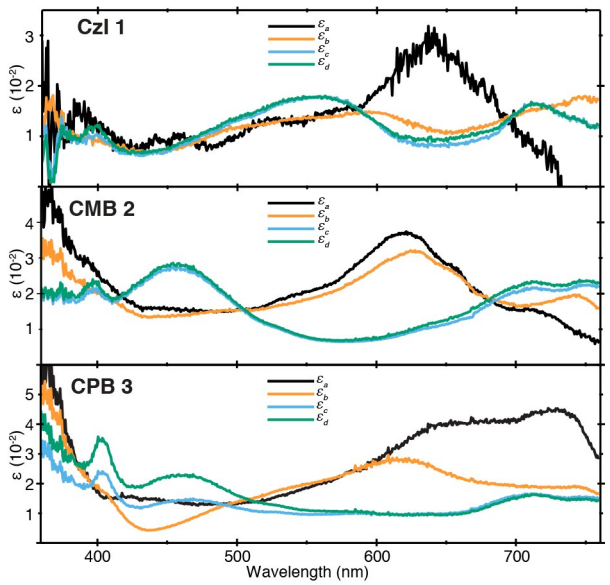

Fig. 10. Evolution-associated difference spectra (ε_i) extracted from the global fit of the ΔA spectra of 1 – 3 in CH_3CN upon excitation at 340 nm.

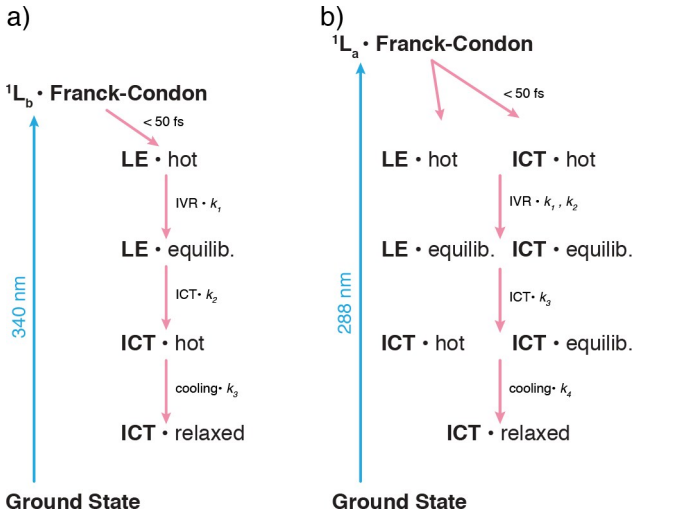

Scheme 1. Kinetic models obtained from the evolution-associated difference global analysis of the transient absorption data measured for **CzI 1**, **CMB 2**, and **CPB 3** in acetonitrile solutions upon a) 340 nm excitation into the S_1 (^1L_b) state and b) 288-nm excitation into the S_2 (^1L_a) state. Intramolecular vibrational energy redistribution (IVR) leads to vibrationally equilibrated (equilib.) solute species in which the excess of vibrational energy is distributed statistically. Vibrational cooling of solutes via energy transfer to solvent leads to relaxed species.

grow. The resulting ΔA spectrum decay somewhat towards 1.2 ns, indicating that the final product states exist on a nanosecond time scale similar to **CzI 1**and **CMB 2**.

The results of global fitting analyses of ΔA spectra and multiexponential fits of ΔA kinetic traces are found to be in mutual agreement, and confirm that all major changes in the 360-720 nm ΔA spectra (λ_{ex} = 340 nm) of **1 – 3** occur before 200 ps. The product states present at 200 ps are too long-lived for the ns decay time constants to be determined from the transient measurements (see Table 3). A satisfactory global fit of the ΔA spectra from 50 fs to 200 ps required a sum of three major evolution-associated difference spectra (ε_i) obeying exponential time dependences (time constants τ_{1g}, τ_{2g}, and τ_{3g}) and a permanent spectrum (Table 4 and Fig. 10). The τ_{1g} component is associated with the blue shift and spectral narrowing of the initial ΔA signals leading to the formation of Bands I at 640, 619 and 614 nm with τ_{1g} = 0.07, 0.10 and 0.11 ps for **1 CzI 1**, **CMB 2**, and **CPB 3**, respectively. The τ_{2g} component describes the decay of Bands I at ~ 620 nm and the rise of Bands II (398, 399 and 404 nm), Bands III (562, 456 and 463 nm) and Bands IV (711, 706 and 713 nm) where τ_{2g} = 1.40, 1.46 and 1.65 ps for **CzI 1**, **CMB 2**, and **CPB 3**, respectively. A third time component is required to account for the rise in the higher energy portion of the Δ*A* spectrum (λ < 590 nm) for **CPB 3** with τ_{3g} = 42 ps. Upon close inspection this third time component is also found for **CzI 1** and **CMB 2** with τ_{3g} = 27 and 36 ps respectively, albeit of much smaller amplitude.

With kinetic data in hand, the following photoinduced dynamics involving the LE and TICT states of carbazol-9-yl benzoic esters **1 – 3** is proposed (Scheme 1a). Excitation at 340 nm corresponds to the carbazole $S_0 \rightarrow {}^1L_b$ transition wherein the excited state is localized on the carbazole ring (LE). As this chromophore is common to all three molecules, **CzI 1**, **CMB 2** and **CPB 3** molecules should exhibit similar transient absorptions in the same spectral range after excitation at 340 nm. Bands I, centered at, 602 nm (**CzI 1**), 624 nm (**CMB 2**) and 614 nm (**CPB 3**), (corresponding to the ε_B spectra in Fig. 10) appear as early as 100 fs after excitation and are thus assigned to absorption from the initially populated, locally excited (LE) states. The preceding spectra, ε_A, are due to vibrationally hot species formed upon the $S_0 \rightarrow {}^1L_b$ excitation. The spectral narrowing and changes observed are typical manifestations of the vibrational relaxation of polyatomic molecules. Intramolecular vibrational energy redistribution (IVR) of large organic molecules takes place within a few hundred fs,[64] which are close to the τ_{1g} values observed. Vibrational cooling of polyatomic molecules in polar solvents, such as acetonitrile, takes place on a longer time scale, typically several picoseconds.[65] The observed τ_{1g} values are also similar to the characteristic solvation time constants in acetonitrile.[66,67] Solvation phenomena are known to cause a blue shift in excited state absorption.[68,69] Therefore, the τ_{1g} time component ($\varepsilon_A \rightarrow \varepsilon_B$) can be assigned to IVR from a non-equilibrated LE state to an equilibrated LE state possibly accompanied by solvation.

The τ_{2g} time component is related to the decay of the LE state species and the formation of a new very long-lived state that is assigned to a TICT state where an electron transfers from carbazole moiety to the isophthalate/benzoate ring moiety (Scheme 2). Bands II (~ 400 nm) and IV (~ 700 nm) are characteristic of the excited-state absorption (ESA) of carbazole cation species (Fig. S26a, ESI†).[25,70,71] The ensuing isophthalate and benzoate radical anion species are expected to absorb in the similar spectral range for **CMB 2** and **CPB 3** but at longer wavelengths in **CzI 1** due to the lower reduction potential. This is in agreement with our observations of Bands III, at 454 and 460 nm bands in **CMB 2** and **CPB 3**, and at lower energies (550 nm) in **CzI 1**. The similar τ_{2g} values observed for **CzI 1**, **CMB 2,** and **CPB 3** indicates that the electronic and

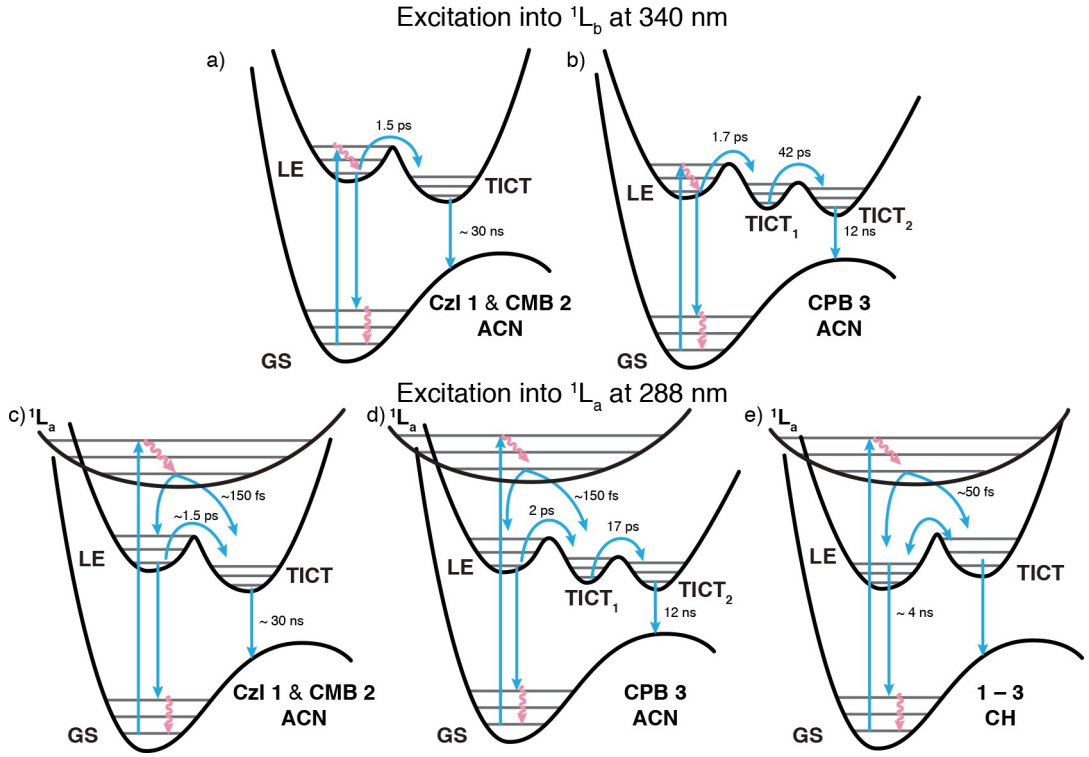

Fig. 11. Jablonski energy level diagrams showing the sequence of states in acetonitrile (ACN) upon excitation at 340 nm for a) **CzI 1** and **CMB 2** and b) **CPB 3**; excitation at 280 nm for c) **CzI 1** and **CMB 2** and d) **CPB 3**; and excitation at 288 nm for **1 – 3** in cyclohexane.

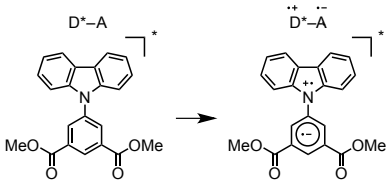

Scheme 2. Photochemical formation of the carbazole radical-cation and isophthalate radical-anion for **CzI 1**.

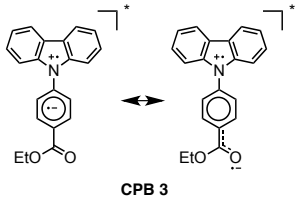

CPB 3

Scheme 3. Hindered rotation of the ester in the excited state of **CPB 3**.

structural factors controlling the electron transfer processes in these related molecules are not that different.

The τ_{3g} component is very pronounced in **CPB 3** but not in **CzI 1** or **CMB 2**. We hypothesize that this component is related to the para- ester carboxylate acceptor. The radical anion of the TICT state, initially formed on the benzoate ring based on excited dipole moments, can be further stabilized by delocalization of charge, via resonance, to a coplanar carbonyl group (Scheme 3). Resonance gives a greater double-bond character to the connecting C–C single bond and torsional motion about this hindered C–C bond should cause the charge to become less dispersed and more localized. This, in turn, should increase the dipole moment and stabilize the energy of the excited state, forming a second ICT state at lower energy (TICT2) (Fig. 11a vs. 11b). The τ_{3g} time constant (42 ps) of **CPB 3** is consistent with hindered rotation with a small potential barrier. The magnitude of the effect is much less pronounced in **CzI 1** and **CMB 2** where the substituent(s) are in *meta*-position(s), and cannot effectively hinder rotation via resonance. Kapturkiewicz *et al*. proposed the existence of similar conformers, based on discrepancies in reorganization energies due to differences in the resultant dipole moments, for carbazoles with aromatic ketone acceptors but with meta-regiochemistry.[27] Unambiguous assignment of the τ_{3g} component to a transition from TICT1 to a second TICT2 requires further synthetic and computational work and is currently in progress.

Excitation at 288 nm In the second measurement set, solutions of **CzI 1**, **CMB 2** and **CPB 3** in acetonitrile were excited at 288 nm, corresponding to the carbazole $S_0 \rightarrow {}^1L_a$ transitions. The initial (0 and 100 fs delay times) ΔA spectra are more congested in comparison to the ΔA spectra measured upon excitation at 340 nm (Fig. 12). Transient absorption bands corresponding to the LE state reached upon excitation at 340 nm are present at 600-620 nm (Bands I) but are much broader. The initial spectra of all three molecules show the broad ~ 400 and ~ 700 nm ΔA bands (Bands II and IV) characteristic of the excited-state absorption for the carbazole

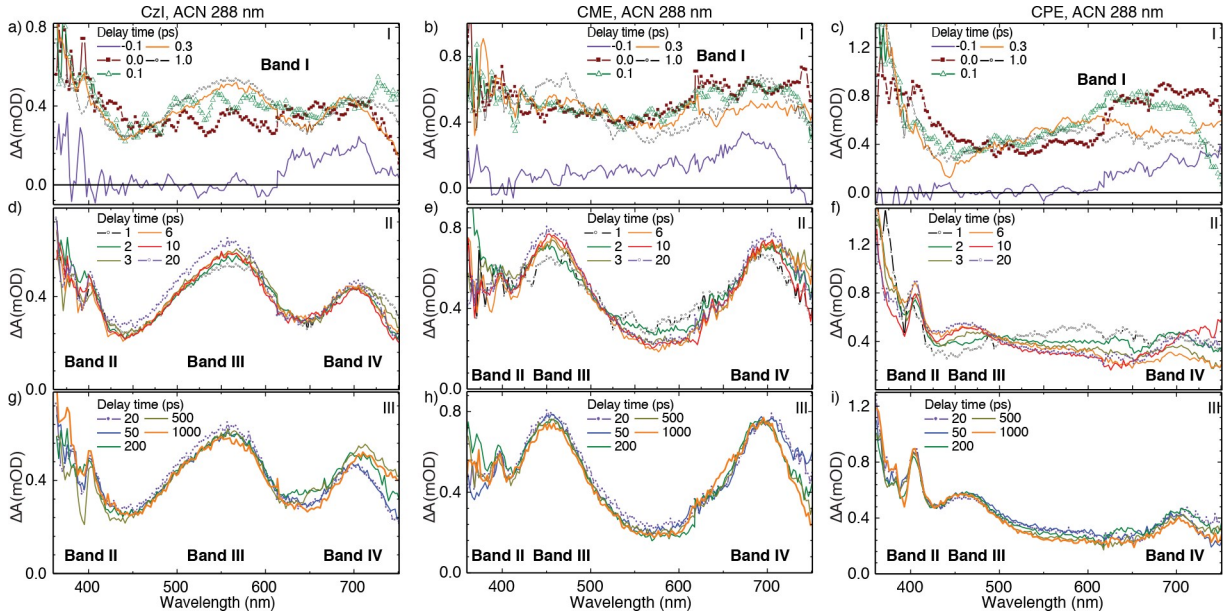

Fig. 12. . Δ*A* spectra of **CzI 1**, **CMB 2**, and **CPB 3** in a 0.1-mm flowing jet of acetonitrile at a – c) 0–1 ps, d – e) 1–20 ps and f– h) 20–1000 ps. Excitation at 288 nm (pulse energy, 2.2 *μ*J). Delay times between the excitation and probe pulses (in picoseconds) are shown in the legends.

cation. The broad visible transient absorptions assigned to isophthalate/benzoate radical anion species (Bands III) are present for **CzI 1** and **CMB 2**. Bands I (600-620 nm) again decay on a 2 ps time scale concomitant with the development of Bands II (~400 nm), Bands III (550, 454 and 460 nm for **CzI 1**, **CMB 2** and **CPB 3**, respectively) and Bands IV (~700 nm) in all three molecules. Bands II – IV undergo some spectral sharpening between 20 and 200 ps and afterwards only minor changes occur up to 1 ns.

Global fit analyses of the ΔA spectra for 288 excitation show four major processes (Fig. S27 in ESI†and Table 4). The first two (τ_{0g} and τ_{1g}) describe ultrafast spectral reshaping of the initial ΔA spectra and have ~ 70 and ~ 170 fs time constants. We note that the τ_{0g}, ε_A and τ_{1g}, ε_B components should be viewed as a guide to the eye rather than the model results for two reasons: (i) these product species are strongly out-of-equilibrium and their absorption line shapes are expected to change with time, in contrast to the presupposition of the constant band shapes by the global fit, and (ii) vibrational relaxation of such highly internally excited species is not necessarily single-exponential but depends on the position of the species within the potential well. The third component (τ_{2g} ~ 1.5 - 2 ps) describes the decay of Bands I (600-620 nm) and the development of Bands II – IV. This component is quite similar to τ_{2g} obtained from 340 nm excitation. At 288 nm, this process is most pronounced in **CPB 3** and least pronounced in **CzI 1**. The fourth and final component, τ_{4g}, corresponds to spectral sharpening of the product bands over several tens of picoseconds.

Taken together, these data paint out the following photoreaction mechanism for the case of 288 nm excitation (Scheme 1b and Fig. 11c,d). For all three molecules, excitation at 288 nm accesses the ^1L_a state of carbazole. Based on Kasha's rule, S_2 is expected to undergo radiationless relaxation into S_1, i.e. $^1L_a \rightarrow {}^1L_b$. The observation of the excited-state absorption from the LE state as early as at the 0-fs delay time between excitation and probe pulses suggests that the radiationless relaxation of the ^1L_a state occurs much faster than the ~ 40 fs pulse duration. At the same delay time, the spectroscopic signatures of the carbazole radical cation (Bands II and IV), characteristic to the formation of the TICT state, are immediately present in all three molecules. Therefore, the decay of the ^1L_a state directly populates the TICT state, in addition to population of the LE. This conclusion is consistent with the steady state excitation spectra (Fig. S12, ESI†). The molecules in the nascent LE and TICT states initially occupy high-energy vibrational levels and the τ_{0g}, ε_A and τ_{1g}, ε_B components likely reflect intramolecular vibrational relaxation of these species. The relaxation of the equilibrated LE state species (τ_{2g}, ε_C) leads to the formation of the hot TICT species, which undergo vibrational cooling (τ_{3g}, ε_D) to produce the relaxed, equilibrated TICT species (ε_E). It is interesting that the immediate observation of the TICT spectroscopic signatures (sub-50 fs) rules out the involvement of any significant twisting motion during the TICT formation. Therefore, any rotation about the C–N bond to achieve the prototypical 90˚ conformation (from the pre-twisted ~50˚) occurs after TICT formation.

Excitation at 288 nm in Cyclohexane Solutions Cyclohexane solutions **CzI 1**, **CMB 2,** and **CPB 3** were excited at 288 nm and transient absorption spectra recorded. These experiments proved to be difficult due to limited solubility of these molecules in cyclohexane solvent and gave decreased signal-to-noise ratio in experimental data. As observed above (Fig. 2), the steady-state emission spectra **CzI 1**, **CMB 2,** and **CPB 3** in

cyclohexane are red-shifted and broadened relative to LE emission observed from **CzP**, which does not form an ICT state.

Transient absorption spectra in all three **CzI 1**, **CMB 2,** and **CPB 3** solutions at short times after 288-nm excitation in cyclohexane (Fig. S28, ESI†) are similar to spectra obtained upon 288 nm excitation of these molecules in acetonitrile (Fig. S26, ESI†). It follows that the interpretation of the spectra is also similar (Scheme 2b and Fig. 11e); 288 nm excitation into the ^1L_a state is followed by ultrarapid (< 50 fs) population of LE and TICT states. The ΔA spectra remain stable until about 200 ps. From 200 ps to 1000 ps, all three molecules behave similarly; ESA bands from the LE (Bands I: ~600 nm) decay, while TICT absorptions of the carbazole cation moiety (Bands II and IV: ~400 and ~700 nm) and the radical anion species (Bands III: ~550 and 450 nm for **CzI 1** and **CMB 2**/**CPB 3**) either decay significantly slower and even rise. This can be interpreted as radiationless relaxation between the LE and TICT states. This relaxation occurs on time scale longer than several hundreds of picoseconds, and possibly occurs in competition with fluorescence. Band integral analysis[72] yields time constants of ca. 2, 4.1 and 3.2 ns for **CzI 1, CMB 2**, and **CPB 3** for the decay process, (Fig. S29, ESI†). Finally, slow decay of the TICT states should follow on a time scale longer than LE. Decay of the TICT state contributes to the observed steady-state emission in CH, apparent as shoulders at longer wavelengths (Fig. S30) but the overall contribution is quite small. Further emission decay profiles were recorded at 390 nm, 425 and 450 nm for **1** and 355, 375 and 410 nm for **3**. The major component was ~4ns for **1** and **3** (consistent with Table 3). Biexponential fitting of emission decays at longer wavelengths (450 and 410 nm, respectively) confirmed the presence of a second component (Fig S31). The contributions of the second component increased with increasing wavelength (from 390 to 450 nm and 355 to 410 nm, respectively) and but the numerical values of these components (4 – 5 ns) were too close to the LE decay (3 – 4 ns, respectively) to be confidently resolved.

Conclusions

This study provides a comprehensive examination of the photophysical processes in the twisted, push-pull carbazol-9-yl benzoic esters **1** – **3**. Dual LE and CT emission is observed in polar and non-polar solvents for meta- benzoic ester **CzI 1** and **CMB 2** whereas only CT emission is observed for the para-benzoic ester **CPB 3**. X-ray crystal structures and DFT calculations support a partially twisted (θ ~ 50˚) ground state that, after photoirradiation, can relax into a fully orthogonal CT excited state. Emission from a decoupled donor-acceptor pair is supported by the dependence of the radiative rate on solvent polarity and small magnitude of the transition dipole moments.

Of particular relevance is the sequence of states in the photochemical ICT reaction deduced from the transient absorption spectroscopy (Fig. 11). Excitation at 340 nm effectively populates the locally excited (LE) ^1L_b states localized on the carbazole chromophore, based on Bands I at ~620 nm in the ΔA spectrum. The LE → TICT photoreaction occurs quickly ($k_{ICT} = 1/\tau_2 = 50 - 70 \times 10^{10}$ s^{-1}) for **1** – **3** and the resultant TICT state slowly decays on the nanosecond time scale. A second TICT state is clearly observed for **CPB 3** and is ascribed to torsional motion between the ester carbonyl and phenyl ring. Higher carbazole-localized excited states, e.g. the ^1L_a state, are reached upon excitation at 288 nm, which rapidly (≤ 40 fs) relax into both LE ^1L_b and TICT states simultaneously.

In summary, these results indicate that rigidification of push-pull chromophores (i.e. in MOFs or solid matrices) should not preclude the rapid LE → TICT photoreaction, which can occur even when the donor-acceptor pairs are weakly coupled, e.g. a pre-twisted θ ~ 45˚. Rather, any enhancement of solid-state emission should arise from suppression of non-radiative decay pathways, which likely involve torsional motion.[73]

Experimental Section

Materials

The synthesis of dimethyl 5-(9H-carbazol-9-yl)isophthalate **1** has been described previously.[14] The new ethyl 3-(9H-carbazol-9-yl)benzoate **2** and ethyl 4-(9H-carbazol-9-yl)benzoate **3** were prepared from carbazole and ethyl 3-iodobenzoate and ethyl 4-iodobenzoate, respectively, using standard Copper cataly8zed Ullman procedures[74] in good yields, 64% for **2** and 70% for **3**. N-phenyl-carbazole **CzP** was prepared from carbazole and bromobenzene. All compounds were purified with flash column chromatography on silica and recrystallized from methanol (**1** and **3**), hexanes (**2**) or ethanol (**CzP**). Compounds were fully characteårized by ^1H and ^{13}C NMR, HIRES mass spectrometry and elemental analysis. Synthesis details are included in the supporting information. Spectroscopic quality cyclohexane (CH), diethyl ether (Et_2O) tetrahydrofuran (THF), dichloromethane (DCM), acetonitrile (ACN), and ethanol (EtOH) was purchased from EMD millipore and used without further purification.

Absorption and Emission measurements

UV-Vis absorption spectra were recorded with Shimadzu UV-2401 PC spectrophotometer at concentrations of 10^{-5} M. Steady state fluorescence measurements were performed on Horiba Fluorolog FL3-11 spectrofluorometer using a 450 W xenon lamp with computer controlled excitation shutter. Emission spectra were recorded upon excitation at the absorption global maximum (290 nm) for each compound. Excitation spectra were recorded at the emission maximum. Lifetime decays were measured using time-correlated single photon counting (TCSPC) with a 340 nm NanoLED excitation source. Absolute quantum yields were measured at Hamamatsu absolute Pl quantum yield spectrometer C11347. Measurements were repeated on multiple (6+) freshly prepared solutions and observed standard deviations are reported. All solutions were deaerated by bubbling nitrogen gas for 15 minutes.

Transient Absorption Measurements

The set-up used in this work is based on a 35-fs regeneratively amplified Ti:sapphire laser system (Spitfire Pro, Spectra-Physics, 1 kHz), the output of which is split to a pump TOPAS-C optical parametric amplifier to produce 288 and 340 nm excitation pulses and to a pump CaF_2 window to produce a white-light continuum probe spanning from 345 to 760 nm (See ESI for a full description). The solutions were circulated through a flowing jet with a 0.1-mm path thickness. The zero delay time is obtained from the non-resonant electronic response from neat solvents measured at the same experimental conditions.[75] The typical excitation energy was 5.3 μJ pulse^{-1} and the linearity of solute Δ*A* signals with excitation energy confirmed that single-photon excitation is responsible for the measured data. The polarization of the excitation beam was set at the magic angle (54.7°) with respect to that of the probe beam. All experiments were performed at 21°C.

Multiexponential fits of ΔA kinetic traces and evolution-associated global fits[76] of ΔA spectra were employed to characterize the temporal evolution of the reactive species in acetonitrile and cyclohexane. Solvent transient absorption signals[75,77] persisted only for 50 fs after excitation and were much smaller than signals from solutes: nevertheless, the 0-50 fs region was excluded from fitting. The ΔA kinetic traces were fitted to a sum of exponential functions:

$$\Delta A = \Delta A_0 + \sum_i A_i e^{-t/\tau_i} \qquad (4)$$

where τ_i are the time constants, A_i are the amplitudes, ΔA_0 is the permanent spectrum at infinitely long times (>> 1 ns). Also, the ΔA spectra were globally fitted to a sum of exponents

$$\sum_j a_j(\lambda)^{-t/\tau_{j,g}} \qquad (5)$$

where $\tau_{j,g}$ are the time constants, and $a_j(\lambda)$ are the decay-associated spectra characteristic of the $\tau_{j,g}$ time components. From these data, the evolution-associated difference spectra ($\varepsilon_j(\lambda)$ or EADS, see p 97 in ref [76]) were reconstructed from based on the assumption of a consecutive reaction mechanism. The *j*-EADS grows with a *j*-lifetime. The global fit assumes that the product absorption line-shapes do not change with time, which can affect the resulting time constants on a scale of several picoseconds typical of vibrational relaxation in solution.

DFT Calculations

Ground state geometry optimizations were performed using the density functional method B3LYP[78] *in vacuo* with the 6-31G* basis set.[79] The absence of imaginary frequencies for fully optimized ground state geometries of **1**-**3** was confirmed by second derivative (Hessian) analysis. Molecular orbital contour plots were visualized with GaussView05.

Acknowledgements

This work was supported by Bowling Green State University, the BGSU Building Strength program and in part by an allocation of computing time from the Ohio Supercomputer Center. ANT acknowledges NSF support (CAREER CHE-0847707, CHE-0923360 and DMR-1006761). The authors also wish to thank Matthias Zeller for his assistance with the X-ray crystallography of **CMB 2** and **CPB 3**;[51] Hoi Ling Luk for assistance with DFT calculations and Mayokun Ayodele for assistance with GC-MS measurements.

Notes and references

‡ Crystal data for **CMB 2**: $C_{21}H_{17}NO_2$, M_r = 315.36, colourless prism, 0.13 × 0.14 × 0.17 mm, Monoclinic, *P 21/c*, *a, b, c* = 20.7631(5), 3.95300(10), 18.9724(4) *Å*, α, β, γ = 90°, 99.9960(10), 90°, V = 1533.55(6) Å^3, Z = 4, ρ = 1.366 gcm^{-3}, Cu *Kα*, F(000) = 664.0, μ = 0.699 mm^{-1}, t = 100K, $2\theta_{max}$ = 79.282, 3249 unique reflections used, 2697 with $I_o > 2\sigma(I_o)$, Rint = 0.052, 218 parameters, 0 restraints, GoF = 1.062, R = 0.042 [$I_o > 2\sigma(I_o)$], wR2 = 0.095 (all reflections), 0.18 < Δρ < –0.32 e Å^3

1 C. W. Schlenker and M. E. Thompson, in *Unimolecular and Supramolecular Electronics I*, ed. R. M. Metzger, Springer Berlin Heidelberg, Berlin, Heidelberg, 2011, vol. 312, pp. 175–212.
2 P. J. Low, M. A. J. Paterson, D. S. Yufit, J. A. K. Howard, J. C. Cherryman, D. R. Tackley, R. Brook and B. Brown, *J. Mater. Chem.*, 2005, **15**, 2304.
3 L. . Hung and C. . Chen, *Mater. Sci. Eng. R Rep.*, 2002, **39**, 143–222.
4 J. V. Grazulevicius, P. Strohriegl, J. Pielichowski and K. Pielichowski, *Prog. Polym. Sci.*, 2003, **28**, 1297–1353.
5 C.-L. Ho, L.-C. Chi, W.-Y. Hung, W.-J. Chen, Y.-C. Lin, H. Wu, E. Mondal, G.-J. Zhou, K.-T. Wong and W.-Y. Wong, *J Mater Chem*, 2012, **22**, 215–224.
6 P. Strohriegl, D. Wagner, P. Schrögel, S. T. Hoffmann, A. Köhler, U. Heinemeyer and I. Münster, eds. F. So and C. Adachi, 2013, p. 882906.
7 B. W. D'Andrade and S. R. Forrest, *Adv. Mater.*, 2004, **16**, 1585–1595.
8 K. Brunner, A. van Dijken, H. Börner, J. J. A. M. Bastiaansen, N. M. M. Kiggen and B. M. W. Langeveld, *J. Am. Chem. Soc.*, 2004, **126**, 6035–6042.
9 A. van Dijken, J. J. A. M. Bastiaansen, N. M. M. Kiggen, B. M. W. Langeveld, C. Rothe, A. Monkman, I. Bach, P. Stössel and K. Brunner, *J. Am. Chem. Soc.*, 2004, **126**, 7718–7727.
10 S. A. Bagnich, S. Athanasopoulos, A. Rudnick, P. Schroegel, I. Bauer, N. C. Greenham, P. Strohriegl and A. Köhler, *J. Phys. Chem. C*, 2015, **119**, 2380–2387.
11 C. J. Gleason, J. M. Cox, I. M. Walton and J. B. Benedict, *CrystEngComm*, 2014, **16**, 7621–7625.
12 V. Jankus, C. Winscom and A. P. Monkman, *J. Chem. Phys.*, 2009, **130**, 074501.
13 S. A. Jenekhe and J. A. Osaheni, *Science*, 1994, **265**, 765–768.
14 L. M. Lifshits, B. C. Noll and J. K. Klosterman, *Chem. Commun.*, 2015, 11603–11606.
15 L. M. Lifshits, C. Campana and J. K. Klosterman, *Acta Crystallogr. Sect. E Crystallogr. Commun.*, 2015, **71**, m152–m153.
16 W. Rettig and M. Zander, *Chem. Phys. Lett.*, 1982, **87**, 229–234.
17 W. Rettig, *J. Mol. Struct.*, 1982, **84**, 303–327.
18 W. Rettig and M. Zander, *Z Naturforsch*, 1984, **39a**, 41–48.
19 N. Mataga, H. Yao, T. Okada and W. Rettig, *J. Phys. Chem.*, 1989, **93**, 3383–3386.
20 J. Dobkowski, Z. R. Grabowski, J. Waluk, W. Kühnle, W. Rettig, C. Rullière, W. Yang, J. Adamus and J. Gebicki, .
21 D. Nie, Z. Bian, A. Yu, Z. Chen, Z. Liu and C. Huang, *Chem. Phys.*, 2008, **348**, 181–186.
22 C. Zhang, L. Feng and Z. Chen, *Chem. Phys. Lett.*, 2006, **420**, 330–335.

23 J. Catalán, C. Díaz, V. López, P. Pérez and R. M. Claramunt, *J. Phys. Chem.*, 1996, **100**, 18392–18398.
24 Y. Mo, F. Bai and Z. Wang, *J. Photochem. Photobiol. Chem.*, 1995, **92**, 25–27.
25 V. A. Galievsky, S. I. Druzhinin, A. Demeter, P. Mayer, S. A. Kovalenko, T. A. Senyushkina and K. A. Zachariasse, *J. Phys. Chem. A*, 2010, **114**, 12622–12638.
26 T. Yoshihara, V. A. Galievsky, S. I. Druzhinin, S. Saha and K. A. Zachariasse, *Photochem. Photobiol. Sci.*, 2003, **2**, 342.
27 A. Kapturkiewicz and J. Nowacki, *J. Phys. Chem. A*, 1999, **103**, 8145–8155.
28 A. Kapturkiewicz, J. Herbich, J. Karpiuk and J. Nowacki, *J. Phys. Chem. A*, 1997, **101**, 2332–2344.
29 A. Kapturkiewicz, J. Herbich and J. Nowacki, *Chem. Phys. Lett.*, 1997, **275**, 355–362.
30 J. Herbich, A. Kapturkiewicz and J. Nowacki, *Chem. Phys. Lett.*, 1996, **262**, 633–642.
31 G. E. Johnson, *J. Phys. Chem.*, 1974, **78**, 1512–1521.
32 R. W. Bigelow and G. E. Johnson, *J. Chem. Phys.*, 1977, **66**, 4861.
33 N. Berman, C. Ruof and H. Howard, *Anal. Chem.*, 1951, **23**, 1882–1883.
34 Sadtler Research Laboratories and W. W. Simons, Eds., *The Sadtler handbook of ultraviolet spectra*, Sadtler Research Laboratories, Philadelphia, Pa, 1979.
35 J. Hicks, M. Vandersall, Z. Babarogic and K. B. Eisenthal, *Chem. Phys. Lett.*, 1985, **116**, 18–24.
36 Z. R. Grabowski, K. Rotkiewicz and W. Rettig, *Chem. Rev.*, 2003, **103**, 3899–4032.
37 E. Lippert, *Z. Für Naturforschung A*, 1955, **10**.
38 N. Mataga, Y. Kaifu and M. Koizumi, *Bull. Chem. Soc. Jpn.*, 1956, **29**, 465–470.
39 L. Onsager, *J. Am. Chem. Soc.*, 1936, **58**, 1486–1493.
40 C. Reichardt, *Solvents and solvent effects in organic chemistry*, Wiley-VCH, Weinheim, 3rd, updated and enl. ed., 2003.
41 J. Karpiuk, Y. N. Svartsov and J. Nowacki, *Phys. Chem. Chem. Phys.*, 2005, **7**, 4070.
42 R. S. Butler, P. Cohn, P. Tenzel, K. A. Abboud and R. K. Castellano, *J. Am. Chem. Soc.*, 2009, **131**, 623–633.
43 J. R. Lakowicz, *Principles of fluorescence spectroscopy*, Springer, New York, 3rd ed., 2006.
44 Y. Niko, S. Kawauchi and G. Konishi, *Chem. - Eur. J.*, 2013, **19**, 9760–9765.
45 N. J. Turro, *Modern molecular photochemistry*, Univ. Science Books, Sausalito, Calif, 1991.
46 M. Maus, W. Rettig, D. Bonafoux and R. Lapouyade, *J. Phys. Chem. A*, 1999, **103**, 3388–3401.
47 S. Sasaki, K. Hattori, K. Igawa and G. Konishi, *J. Phys. Chem. A*, 2015, **119**, 4898–4906.
48 J. Herbich and A. Kapturkiewicz, *Chem. Phys.*, 1991, **158**, 143–153.
49 J. Herbich and A. Kapturkiewicz, *Chem. Phys.*, 1993, **170**, 221–233.
50 S. Murali, V. Kharlanov, W. Rettig, A. I. Tolmachev and A. V. Kropachev, *J. Phys. Chem. A*, 2005, **109**, 6420–6429.
51 L. M. Lifshits, M. Zeller and J. K. Klosterman, *Manuscript in Preparation.*
52 L.-Q. Chen, C.-L. Yang, X.-G. Meng and J.-G. Qin, *Acta Crystallogr. Sect. E Struct. Rep. Online*, 2005, **61**, o3073–o3075.
53 S. Saha and A. Samanta, *Acta Crystallogr. C*, 1999, **55**, 1299–1300.
54 C. Avendaño, M. Espada, B. Ocaña, S. García-Granda, M. del R. Díaz, B. Tejerina, F. Gómez-Beltrán, A. Martínez and J. Elguero, *J Chem Soc Perkin Trans 2*, 1993, 1547–1555.
55 Y.-Z. Xie, J.-Y. Jin and X.-C. Qu, *Acta Crystallogr. Sect. E Struct. Rep. Online*, 2012, **68**, o1199–o1199.
56 A. L. Hickey and C. N. Rowley, *J. Phys. Chem. A*, 2014, **118**, 3678–3687.
57 A. G. Pinkus and E. Y. Lin, *J. Mol. Struct.*, 1975, **24**, 9–26.
58 A. R. Katritzky, M. V. Sinnott, T. T. Tidwell and R. D. Topsom, *J. Am. Chem. Soc.*, 1969, **91**, 628–636.
59 E. N. Gur'yanova and N. . Grishko, *Zhurnal Strukt. Khimii*, 1963, **4**, 368–71.
60 C. J. Jödicke and H. P. Lüthi, *J. Am. Chem. Soc.*, 2003, **125**, 252–264.
61 E. K. U. Gross and W. Kohn, in *Advances in Quantum Chemistry*, Elsevier, 1990, vol. 21, pp. 255–291.
62 M. E. Casida, *J. Mol. Struct. THEOCHEM*, 2009, **914**, 3–18.
63 R. D. Amos, *Chem. Phys. Lett.*, 2002, **364**, 612–615.
64 T. Elsaesser and W. Kaiser, *Annu. Rev. Phys. Chem.*, 1991, **42**, 83–107.
65 I. Martini and G. V. Hartland, *J. Phys. Chem.*, 1996, **100**, 19764–19770.
66 M. Maroncelli, *J. Mol. Liq.*, 1993, **57**, 1–37.
67 M. L. Horng, J. A. Gardecki, A. Papazyan and M. Maroncelli, *J. Phys. Chem.*, 1995, **99**, 17311–17337.
68 P. F. Barbara and W. Jarzeba, in *Advances in Photochemistry*, eds. D. H. Volman, G. S. Hammond and K. Gollnick, John Wiley & Sons, Inc., Hoboken, NJ, USA, 1990, pp. 1–68.
69 R. Jimenez, G. R. Fleming, P. V. Kumar and M. Maroncelli, *Nature*, 1994, **369**, 471–473.
70 T. Ueda, R. Fujisawa, H. Fukumura, A. Itaya and H. Masuhara, *J. Phys. Chem.*, 1995, **99**, 3629–3635.
71 H. Miyasaka, T. Moriyama, S. Kotani, R. Muneyasu and A. Itaya, *Chem. Phys. Lett.*, 1994, **225**, 315–321.
72 T. Bultmann and N. P. Ernsting, *J. Phys. Chem.*, 1996, **100**, 19417–19424.
73 D. A. Shultz and M. A. Fox, *J. Am. Chem. Soc.*, 1989, **111**, 6311–6320.
74 C. Sambiagio, S. P. Marsden, A. J. Blacker and P. C. McGowan, *Chem. Soc. Rev.*, 2014, **43**, 3525.
75 S. A. Kovalenko, A. L. Dobryakov, J. Ruthmann and N. P. Ernsting, *Phys. Rev. A*, 1999, **59**, 2369–2384.
76 I. H. M. van Stokkum, D. S. Larsen and R. van Grondelle, *Biochim. Biophys. Acta BBA - Bioenerg.*, 2004, **1657**, 82–104.
77 M. Rasmusson, A. N. Tarnovsky, E. Åkesson and V. Sundström, *Chem. Phys. Lett.*, 2001, **335**, 201–208.
78 C. Lee, W. Yang and R. G. Parr, *Phys. Rev. B*, 1988, **37**, 785–789.
79 R. Ditchfield, *J. Chem. Phys.*, 1971, **54**, 724.